ARTICLE

Using Metallic Noncontact Atomic Force Microscope Tips for Imaging Insulators and Polar Molecules: Tip Characterization and Imaging Mechanisms

David Zhe Gao,[†,*] Josef Grenz,[‡] Matthew Benjamin Watkins,[†] Filippo Federici Canova,[†,§] Alexander Schwarz,[‡,*] Roland Wiesendanger,[‡] and Alexander L. Shluger[†,§]

[†]Department of Physics and Astronomy, University College London, Gower Street, London WC1E 6BT, United Kingdom, [‡]Institute of Applied Physics, University of Hamburg, Jungiusstr. 11, 20355 Hamburg, Germany, and [§]WPI-AIMR, Tohoku University, 2-1-1 Katahira, Aoba-ku, Sendai 980-8577, Japan

ABSTRACT We demonstrate that using metallic tips for noncontact atomic force microscopy (NC-AFM) imaging at relatively large (>0.5 nm) tip−surface separations provides a reliable method for studying molecules on insulating surfaces with chemical resolution and greatly reduces the complexity of interpreting experimental data. The experimental NC-AFM imaging and theoretical simulations were carried out for the NiO(001) surface as well as adsorbed CO and Co-Salen molecules using Cr-coated Si tips. The experimental results and density functional theory calculations confirm that metallic tips possess a permanent electric dipole moment with its positive end oriented toward the sample. By analyzing the experimental data, we could directly determine the dipole moment of the Cr-coated tip. A model representing the metallic tip as a point dipole is described and shown to produce NC-AFM images of individual CO molecules adsorbed onto NiO(001) in good quantitative agreement with experimental results. Finally, we discuss methods for characterizing the structure of metal-coated tips and the application of these tips to imaging dipoles of large adsorbed molecules.

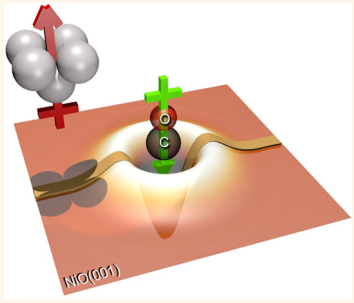

KEYWORDS: NC-AFM · insulator · imaging mechanism · metallic tip · virtual AFM

Understanding the mechanisms of adsorption, interaction, and assembly of atoms and molecules on insulating surfaces is critical to many areas of surface science, such as catalysis,[1] lubrication,[2,3] and molecular electronics.[4−6] Studies of individual molecules, molecular aggregates, and more complex structures at insulating surfaces often involve noncontact atomic force microscopy (NC-AFM).[7−17] However, the interpretation of experimental images is difficult, and systematic high-resolution studies of individual molecules are still rare. It is widely acknowledged that knowing the structure of the NC-AFM tip apex is vital for our understanding and faithful interpretation of high-resolution NC-AFM images.[18,19] Using well-characterized, stable, and atomically sharp tips is essential for achieving atomic resolution when imaging molecules at surfaces and for accurately analyzing the experimental data. However, preparing such tips is still a matter of trial and error.

Solving this problem requires developing ways of characterizing and controlling the tip atomic structure. One strategy has been to characterize tips using field ion microscopy (FIM);[20] however, it is not practical to analyze every tip used before and after measurements. A possible solution to the tip control problem is to functionalize the tip using a small molecule, such as CO,[21] or a Xe atom.[22] In many sample systems, however, controlled functionalization of the AFM tip is difficult to achieve. The imaging strategy with such tips has been based on measuring short-range repulsion forces,[23] which has both advantages (it provides intramolecular resolution) and disadvantages (it may distort the image or manipulate mobile molecules).

* Address correspondence to david.gao.10@ucl.ac.uk, aschwarz@physnet.uni-hamburg.de.

Received for review April 1, 2014 and accepted May 1, 2014.

Published online May 01, 2014
10.1021/nn501785q

Microfabricated Si cantilevers with integrated pyramidal Si tips are widely used in NC-AFM experiments. Due to the presence of directional covalent bonds, Si or oxidized Si tip apexes exhibit many possible tip structures. Thus, many different tip models need to be tested to find reasonable agreement between experiment and simulation.[24] On the other hand, atomically sharp stable metallic tip apexes, which allow for atomic resolution, can be expected to have a pyramid-like pointed structure.[25] We have recently observed that Cr-coated Si tips provide good atomic resolution with chemical specificity when imaging is carried out at rather large (>0.5 nm) tip−surface separations on binary ionic surfaces.[26−29] Such tips can be prepared *via* thermal evaporation *in situ*.[26] Moreover, the conductivity of the coated tip can be checked to ensure that it is indeed metallic.[27] Recently, this method has been used to determine the adsorption site and geometry of single Co-Salen molecules on the NaCl(001)[28] and NiO(001)[29] surfaces with atomic accuracy. These metallic tips can be used to atomically resolve flat surfaces at large distances with minimal risk of contamination from the surface. The high chemical resolution achieved on these ionic substrates has been attributed to the existence of a dipole moment at the metallic tip apex. However, the magnitude and origin of this dipole are still poorly understood.

The mechanisms responsible for chemical contrast when employing metallic tips has been attributed to the Smoluchowski effect.[30] It is generally accepted that step features at metal surfaces possess dipole moments due to the incomplete screening of positive ion cores by conduction electrons. This is consistent with measurements studying the influence of step edge density on work function performed on the Au(111),[31] Cu(111),[31] Pt(111),[32] and W(110)[32] surfaces, which all indicated the presence of a 0.1−0.2 D dipole moment. Calculations using the jellium model predict that this dipole is proportional to step height and screening length.[33] However, the magnitudes of dipole moments observed at step edges appear to be too small for the presence of these features to explain the experimentally observed image contrast at large tip−surface separations. The occurrence of larger dipole moments at the tip apex requires sharper, pyramidal features,[27] possessing lower coordinated atoms. The existence of such features can be inferred from NC-AFM and other experiments but cannot be proven by directly imaging the tip.

In this work, we introduce a systematic procedure for characterizing metal-coated tips and imaging molecules at bulk insulator surfaces using NC-AFM. We demonstrate that, by imaging the surface with atomic resolution, one can determine the effective tip dipole moment. Chemical identification of surface ions and images of small adsorbed molecules can be then well-described by using a point dipole to represent the tip. We prove that by comparing experimental and theoretical scan lines of adsorbed CO molecules on NiO(001).

In particular, our results demonstrate that metallic tip apexes are consistent with pyramidal nanoasperities with a typical electric dipole moment on the order of a few Debye (1 D = 3.3×10^{-30} Cm). At distances of 0.5 to 0.8 nm from the surface, such a tip effectively behaves like a point dipole. Irregularly shaped multiasperity tips can be represented as several dipoles. Using such tips can result in artifacts if polar molecules are imaged. The imaging mechanism is therefore easy to model as contrast is primarily due to electrostatic interactions. Once the tip dipole moment is estimated, modeling of surface images from density functional theory (DFT) is reliable and much faster than with conventional methods.[27,34] Although at short tip−surface separations these tips are effectively blunt and cannot resolve the internal structure of larger molecules, they may be able to probe molecular dipole moments. We note that interpretation of NC-AFM images obtained using CO-functionalized tips at large distances[35] is similar to that with metallic nanoasperity tips. This is due to the fact that a CO molecule possesses a dipole moment, as well (although significantly smaller in magnitude than the dipole moment of pyramidal metallic nanotips), which, if adsorbed on a metallic tip, also points with its positive pole toward the surface.

RESULTS

Metallic AFM Tips. Perhaps the closest one can get to characterizing the atomic structures of metallic STM and AFM tips is by using FIM. Tips fabricated from polycrystalline and single-crystalline W(111) wire *via* DC electrochemical etching have been studied in this way before and after using them to image various surfaces.[20] These results demonstrate the presence of atomic steps at the otherwise smooth W tip surface. A number of work function measurements at metal step edges are consistent with the Smoluchowski effect; however, the dipoles inferred are generally much smaller in magnitude than those predicted for Cr-coated AFM tips.[27]

In this work, the entire Si cantilever was coated *in situ* with nominally 4 nm of Cr to produce a conducting path between the tip apex and the cantilever stage. Cr adheres well to the Si oxide layer, and thin Cr films have been used in the past to improve the deposition of other metals[36−38] on oxidized Si. The deposited Cr exposes the (110) surface, and these films are known to be quite rough; their morphology depends on the method of deposition and the film thickness.[36−38]

Previous theoretical studies using a Cr tip model[27] indicated the presence of a dipole moment with the positive end oriented away from the surface. Here we

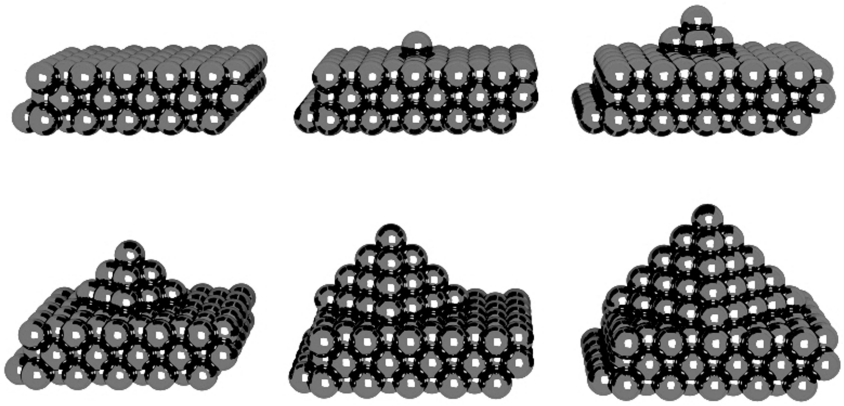

Figure 1. Array of pyramid features ranging from 0 to 5 atomic layers in height constructed on the Cr(110) surface. These pyramid features represent some possible stable atomic structures found on a vapor-deposited Cr tip or surface.

elucidate how this dipole moment depends on the tip morphology and demonstrate that the proposed tip model is consistent with the experimental data.

We approximate our Cr-coated tips as macroscopic spheres terminated by Cr(110) terraces (Cr crystallized in the bcc structure). Representative nanotips were constructed as pyramidal asperities on the Cr(110) surface, as shown in Figure 1. The pyramid structure was chosen according to classic Wulff construction[39] to minimize the total surface energy of the asperity. The total dipole moment of the surface with a pyramidal nanotip was calculated from a change in the work function of the system (see Methods for details). We note that using Cr clusters rather than surface slabs with pyramidal asperities shown in Figure 1 may lead to incorrect predictions.[40]

The dependence of the magnitude of the tip dipole moment on the number of atomic layers in the pyramid is shown in Figure 2. These results agree with prior calculations[27] that predicted 1.2 D for a single adatom and 6 D for a three atom high nanoasperity and are comparable to the experimental measurements on the Au and Cu surfaces.[31] In these experiments, the dipole moment was determined to be 0.16 D/step atom on Au and 0.5 D/step atom on Cu surfaces.[31] While these results present dipole moments that are significantly smaller, they correspond to edge atoms that are better coordinated than single adatoms. It has indeed been previously predicted that the Smoluchowski effect should increase with increasing step height and decreasing coordination.[33] Larger pyramid features containing lower coordinated atoms are expected to possess much larger dipole moments than step edges.

Our results show, however, that the dipole moment of a pyramidal nanotip does not scale linearly with pyramid height. This effect can be explained by the difference in work function between the (110) and (100) surfaces of Cr. The work function of Cr(110) was calculated to be 4.8 eV, while the work function of

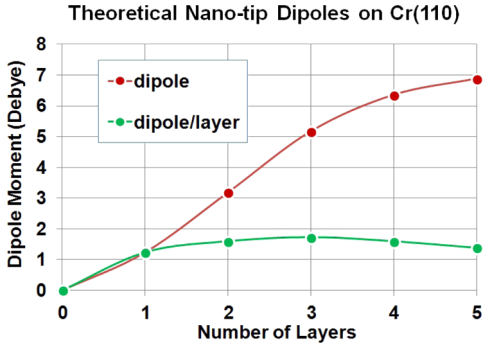

Figure 2. Total dipole moment of various pyramidal nanotips as a function of pyramid height. These tips were constructed as pyramidal asperities on the Cr(110) surface. The dipole moment found at the tip apex of these asperities increases with pyramid size but should eventually converge to a maximum value.

Cr(100) was calculated to be 4.0 eV. As Cr(100) facets are exposed as sides of the pyramid tip on the surface of Cr(110), a charge transfer occurs that contributes to the total dipole moment of the tip. The work function near these asperities decreases until it eventually converges to the value of the Cr(100) surface itself. At this point, the total dipole moment of the tip should converge, as well. This suggests that the Smoluchowski effect is not the only mechanism involved and that charge transfer due to a difference in work function must be considered. It then follows that the dipole moment may be greatly reduced or even inverted in some materials.

To illustrate this point further, we have also considered pyramidal asperities grown on the less stable Cr(100) surface. In this case, one can expect that the surface may transfer charge to the tip apex instead. The dipole moment of several pyramidal asperities grown on Cr(100) are shown in Figure 3. These results show that asperities on less stable surfaces may possess inverted dipole moments due to charge transfer from the surface to the asperity apex. On Cr(110), the orientation of the dipole moment due to charge transfer matches the contribution from the Smoluchowski

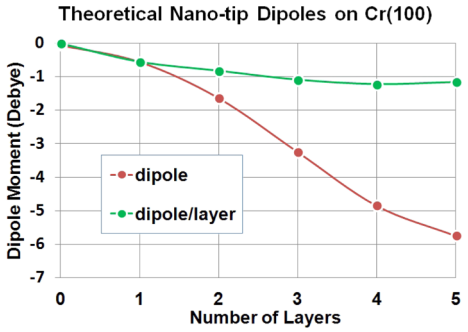

Figure 3. Total dipole moment of a series of pyramidal nanotips on Cr(100) as a function of pyramid height. The work function of the Cr(100) surface is much lower than that of the Cr(110) surface, resulting in charge transfer from the surface to the asperity apex instead.

effect. On Cr(100), however, the two contributions work against each other and result in a lower absolute value of the dipole moment. The magnitude of these dipole moments is indeed on average 1 D lower than those predicted for the Cr(110) surface. Since it is difficult to define the work function of a small facet, this discussion is only qualitative. At the genuine nanoscale, the distinction between these two effects blurs and all that can be considered is the net effect of electron density redistribution around the nanotip.

In the following discussion, we assume that the exposed surfaces in experimentally produced tips are the most stable ones, that is, pyramidal nanotips on Cr(110). Such tips would possess dipole moments with the positive pole oriented toward the surface. We then show that at large tip–surface separations the tip dipole can be represented using a point dipole.

Explicit Calculation of Experimental Tip Dipoles. To further quantify this model, we used the experimental data obtained as a result of imaging the NiO(001) surface with Cr-coated tips. We demonstrate that, assuming the point dipole approximation for a metallic AFM tip, the magnitude and orientation of this dipole can be determined from the experimental data.

The total force can be decomposed into long-range van der Waals (vdW) interactions between the macrotip and the surface, local vdW interactions between the nanotip and the surface, and midrange electrostatic interactions between localized dipoles in the tip and sample, as illustrated in Figure 4. At large tip–sample distances, the contribution from short-range repulsive interactions can be ignored. Note that long-range electrostatic interactions are negligible, as the average contact potential difference is compensated for by applying an appropriate bias voltage between the tip and sample.

At large tip–surface separations, only the forces due to macroscopic vdW interactions are present. This component can be accounted for using an analytical expression and fitting a set of parameters directly to the experimental data. In this simple model, a tip is

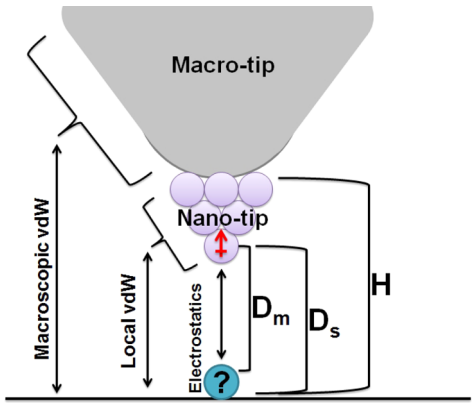

Figure 4. Schematic of the proposed tip model imaging the surface and a small molecule. The main contributions to force are macroscopic vdW interactions, local vdW interactions, and midrange electrostatic interactions. Distance between the macrotip and the surface is defined as *H*, distance between the nanotip and the surface is defined as D_s, and distance between the nanotip and the molecule is defined as D_m.

represented by a conical section with a spherical cap[41] and the force can be calculated with respect to distance between the macrotip and the surface *H*. To achieve that, a long-range theoretical force curve was fit to an experimental force curve measured above the NiO(001) surface and compared in Figure 5. In order to obtain a physically meaningful and unique fit, the parameters of the model were constrained in the context of what we know about our tip and the materials used in the system. The Hamaker constant A_H can be calculated using Lifshitz theory from dielectric constants and refractive indices for a variety of inorganic materials.[42] In our case, we have constrained the value to be within a realistic range of 5×10^{-20} to 60×10^{-20} J. Since the uncoated sharp Si tip had a starting radius of 2.0 nm, the Cr-coated tip radius *R* was constrained within the range of 1.0 to 10.0 nm. Finally,

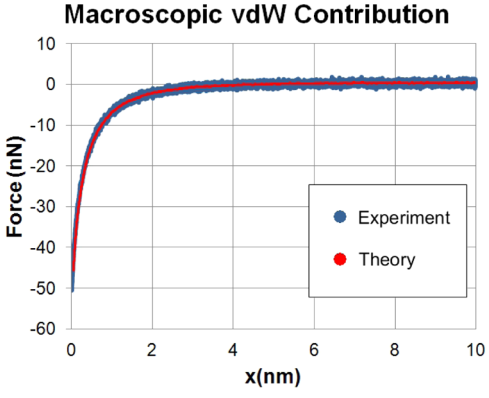

Figure 5. Experimental long-range force curve compared with the theoretical long-range force curve. The mathematical functions used were chosen to physically represent the metal-coated AFM tip.[41] Experimental parameters: f_0 = 186.278 kHz, $c = 144 \pm 21$ N/m, $A_0 = 0.6 \pm 0.1$ nm, $Q = 20996$. Optimized tip model parameters: $A_H = 40 \pm 12 \times 10^{-20}$ J, $R = 4.0 \pm 0.9$ nm, $\gamma = 16.4 \pm 1.2°$.

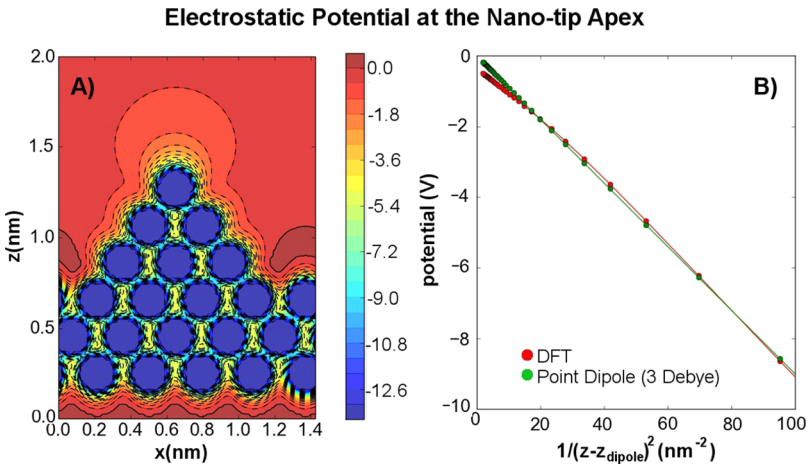

Figure 6. (A) Electrostatic potential of a system containing a three-layer nanoasperity on Cr(110) with a total dipole moment of 5 D. When the isosurface of this electrostatic potential is visualized, a large spherical feature appears above the apex atom that can be interpreted as the positive lobe of a dipole moment. (B) Plot of the electrostatic potential with respect to distance away from the nanotip apex. A 3 D point dipole positioned at the atomic coordinates of the apex atom is able to reproduce the local electrostatic potential obtained from DFT calculations.

since the tip is believed to be quite sharp, the tip cone angle γ was constrained within a range of 0 to 90°. The sample surface plane was defined by taking the average position of atomic nuclei on the NiO(001) surface, and the macrotip to sample distance H was defined as the minimum distance between the surface plane and the macroscopic tip sphere.

Within these constraints, the experimental data can be well-described by $A_H = 40 \pm 12 \times 10^{-20}$ J, $R = 4.0 \pm 0.9$ nm, and γ of 16.4 $\pm$ 1.2°. Using these parameters, we were then able to extrapolate the absolute height H of the macroscopic tip at a given Δf from the theoretical force curve.

The second major contribution to the total force comes from the electrostatic interaction between localized charges present in the metallic tip and the sample. Note that this very local electrostatic interaction is not nullified when compensating for the long-range average contact potential difference. This interaction determines the image contrast when the nanotip to surface distance D_s is between 0.5 and 1.0 nm. In order to estimate the value and position of the dipole moment, we examined the electrostatic potential near a three-layer Cr nanotip on the Cr(110) surface, as shown in Figure 6.

A contour plot of the electrostatic potential obtained from DFT calculations depicted in Figure 6A shows a spherical feature above the asperity, which may be interpreted as the positive lobe of a dipole moment. According to Figure 2, the total dipole moment of a three-layer pyramidal nanotip is 5 D. However, the local electrostatic potential near the tip apex can be reproduced by positioning a 3 D point dipole at the apex atom, as shown in Figure 6B. The interaction between this point dipole and the electrostatic potential of the sample is then obtained from DFT calculations. Finally, we produce the macroscopic vdW + electrostatic force field and use the virtual AFM (vAFM)[34] code to simulate NC-AFM scan lines at the experimental parameters of AFM operation. The vAFM code integrates the equation of motion of the cantilever and models feedback circuits found in a real apparatus, providing full simulation of the real experiment.

The final possible contribution to total force in our model comes from local vdW interactions between the nanotip and the surface, which can be computed using a semiempirical method.[43] Since this contribution is heavily dependent on the precise atomic structure of the nanotip, which cannot be deduced from experimental data, we do not include these interactions in our initial vAFM simulations. Their importance is analyzed afterward to gain insight into the differences between theoretical and experimental images.

Experimentally, we have measured NC-AFM images with atomic resolution of the bare NiO(001) surfaces using the same cantilever as in Figure 5. Twenty-three scan lines in the [100] direction from one such image were averaged to obtain the mean atomic corrugation amplitude. The dipole moment at the tip and the height of the nanoasperity were then fit to reproduce this scan line, as shown in Figure 7. The height of the macrotip H (see Figure 5) required to produce the experimental Δf of -50 Hz was calculated to be 1.24 nm. Point dipoles from 1 to 20 D were then placed at various positions corresponding to the apex atoms of asperities consisting of 1−5 atomic layers. The best fit was achieved with a tip dipole moment of 7 D positioned at the tip apex of a three atomic layer high nanoasperity (0.6 nm away from the macrotip). The theoretical noise in the calculated scan line is due to the digital phase lock loop and the integration time step employed within the vAFM.

Although the agreement between experimental and theoretical scan lines for this dipole moment value

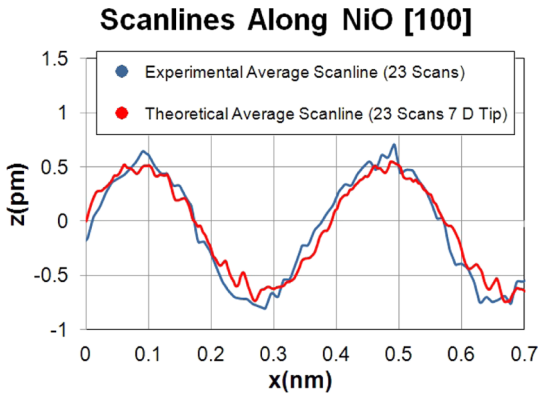

Figure 7. Experimental and theoretical scan lines above the bare NiO(001) surface in the [100] direction. The theoretical scan line was generated using a 7 D dipole moment and compared to the experimental average scan line. Experimental parameters: same as in Figure 5, $\Delta f = -50$ Hz.

is remarkably good, we note that the magnitude and position of the point dipole are inter-related and cannot be uniquely defined. They provide only plausible information about the actual atomic structure of the tip. The local vdW interactions between the nanotip and the surface will differ, depending on the exact structure of the nanotip. In the distance regime proposed here, for a three-layer pyramidal nanotip model, this contribution to the image contrast is negligible and therefore not considered. At smaller nanotip to surface distances D_s, however, these interactions will become important.

These results demonstrate that, at relatively large tip−surface separations, a Cr-coated tip can be consistently represented by a conical macroscopic tip terminated by a sphere and a pyramidal nanotip consisting of several atomic layers with a dipole moment of a few Debye. Out of 36 metal-coated tips, 26 were observed to possess sufficiently large dipole moments and were capable of atomic resolution. In the other nine cases, the tip was either too blunt or not metallic. We now show that this model also allows us to provide quantitative interpretation of NC-AFM images of CO molecules adsorbed at the NiO(001) surface.

Imaging the CO Molecule. An ultimate test of this model would be to compare theoretical scan lines using the point dipole approximation with experimental scan lines and images of small molecules, such as CO, on the NiO(001) surface. CO molecules were deposited onto the NiO(001) surface and imaged using the same Cr-coated tip as the one used to obtain atomic resolution on the surface (see Figure 7) and record long range forces (see Figure 5). A large number of bright rings with central depressions (donuts), corresponding to individual CO molecules, can be seen in constant Δf images of the surface after deposition of CO, as shown in Figure 8A. Figure 8B shows scan lines over the centers of 60 CO molecules on NiO(001) in the [100] direction. These were then averaged to generate a mean scan line to compare with theoretical predictions using the same point dipole model parameters that reproduced the atomically resolved data on NiO(001) in the previous section.

DFT calculations of the CO molecule predict a 0.1 D dipole moment in the gas phase with the positive pole at the O atom. The CO molecule then adsorbs perpendicular to the surface with the C atom above a surface Ni ion and an adsorption energy of 0.3 eV. In the adsorbed state, the CO dipole moment increases to 0.4 D with its positive end pointing away from the surface. The molecule is tilted 6° toward a Ni atom with Ni−C contributing 2° and C−O contributing 4°. This is qualitatively in agreement with prior theoretical predictions[44,45] and within the error range of experimental estimates[46] of 12 ± 12°. This small tilt could be observable with a point dipole tip if vAFM images are generated from static DFT calculations performed at 0 K. However, due to high surface symmetry, there are four energetically equivalent configurations that must be considered. Transitions between these configurations occur through the purely upright configuration with an energy barrier of only 0.006 eV, which is within the error range of DFT and may be interpreted as

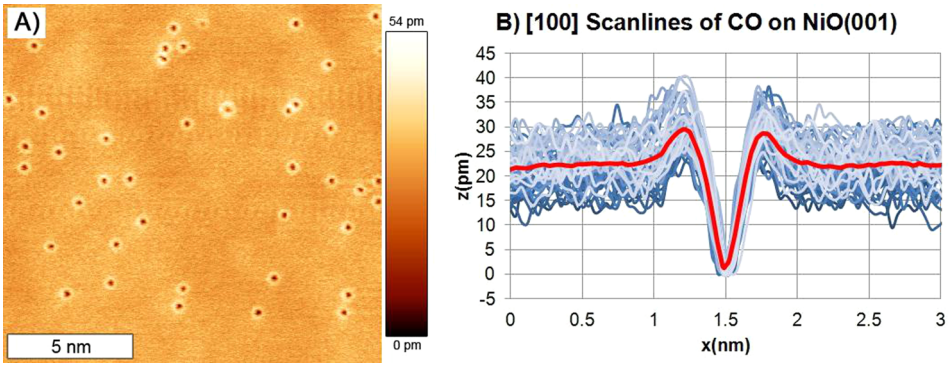

Figure 8. (A) CO molecules on the NiO (100) surface imaged at 8 K as bright rings with a central depression (donuts). (B) Sixty scan lines above CO molecules along the [100] direction and a representative average scan line. Experimental parameters: same as in Figure 5, $\Delta f = -48$ Hz.

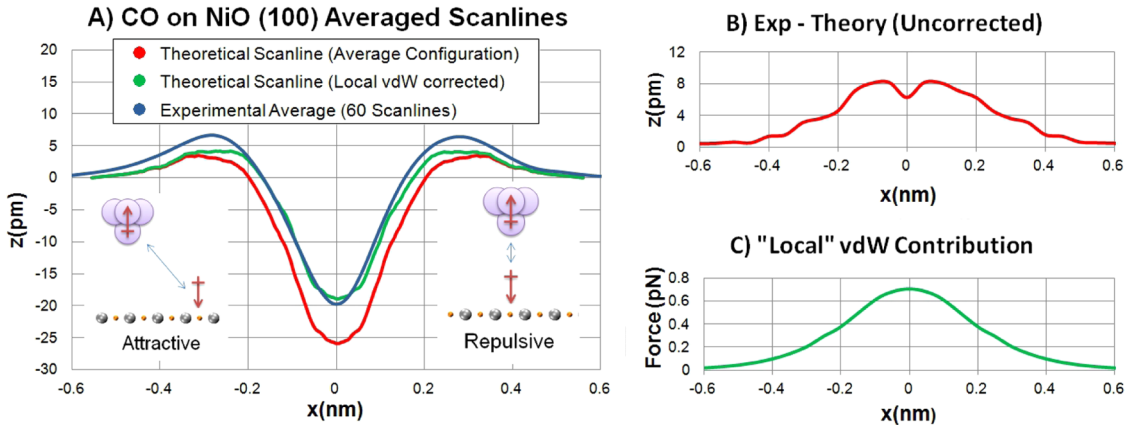

Figure 9. (A) Experimental and theoretical scan lines of CO adsorbed onto the NiO(001) surface in the [100] direction. The theoretical long-range forces were fit to experimental data, and the tip was represented as a 7 D point dipole 0.6 nm below the macrotip. The experimental scan line (red averaged scan line shown in Figure 8B) was produced by averaging over the data for 60 CO molecules on the NiO surface, and the theoretical scan line was produced by averaging over four energetically equivalent tilted states on the surface as well as the upright configuration. Including local vdW interactions improves agreement with experiment. (B) Difference between experimental and uncorrected theoretical scan lines with $x = 0$ representing the center of the CO molecule. (C) Local vdW interactions between the pyramidal nanotip scanning 0.46 nm above a CO molecule. This contribution was computed using a semiempirical scheme[43] assuming an upright configuration for CO.

negligible. Furthermore, molecular dynamics simulations performed at 8 K estimate that the attempt frequency for switching between these equivalent states is 10^{13} Hz. Therefore, the molecule is rapidly switching between equivalent tilted configurations. Since AFM scan rates are many orders of magnitude slower than the switching frequency of CO on the surface, an average of the upright configuration and four equivalent tilted configurations must be considered when producing vAFM images or scan lines.

When the AFM tip approaches a CO molecule on the surface, there is an attraction due to lateral interactions between the tip and molecule, as shown in Figure 9A. This interaction is responsible for the bright rings in the image. However, when the dipole of the tip and the CO molecule on the surface are nearly on top of each other and aligned with the positive ends pointed toward each other, the resulting local repulsive interaction is responsible for the dark spot within the bright rings.

The experimental scan line over an adsorbed CO molecule averaged over 60 scan lines and a theoretical scan line obtained using vAFM are compared in Figure 9A. The theoretical scan line was calculated using the model of the tip–surface vdW interaction described in the previous section. A 7 D point dipole positioned 0.6 nm below the macrotip was used to represent the Cr-coated tip and the electrostatic potential of the CO molecule on the NiO(001) surface was obtained from DFT calculations of the adsorbed system. The absolute minimum distance between the CO molecule and the nanotip (D_m) in this case was calculated to be 0.46 nm. The corresponding minimum distance between the nanotip and the NiO(001) surface (D_s) is 0.78 nm. At this tip–surface distance, atomic resolution of the surface should no longer be possible, in agreement with experimental data.

Theory predicts that the CO molecule is observed as a bright ring with a dark spot indicating repulsion at the center. Since surface atoms can no longer be resolved at this tip–sample distance, the surface level can simply be defined as the cantilever height far away from the CO molecule. The bright ring is 3 pm above the surface level, while the depression is 26 pm below the surface level. The diameter of the ring is 0.6 nm in this case and defined as the horizontal distance between maxima on opposite sides of the bright ring. Averaged experimental scan lines give a similar bright ring 6 pm above the surface level with a standard deviation of 3 pm and an average depression that lies 20 pm below the surface level with a standard deviation of 2.5 pm. The experimental diameter of the bright ring was observed to be 0.52 nm with a standard deviation of 4 pm. The total size of the CO molecule is about 1.5 nm in both theory and experiment. Furthermore, the average height difference between maxima on opposite sides of the molecule is only 0.7 pm with a standard deviation of 2.2 pm. This indicates that the height of the ring is constant along the entire perimeter and that the dipole moment of the tip is therefore oriented nearly perpendicular with respect to the surface plane. Since the total size of the CO molecule is identical in experiment and simulation, tip convolution effects are negligible, indicating an atomically sharp tip.

The difference between the experimental and theoretical scan lines is shown in Figure 9B. The largest discrepancy is found near the center of the CO molecule and falls off with increasing distance. This difference may be accounted for by examining the vdW interactions between the CO molecule and the pyramidal nanotip. Since this contribution is always

attractive, it would reduce the depth of the depression and increase the height of the ring. Local vdW interactions between a pyramidal nanotip scanning 0.78 nm (D_s) above the surface and an adsorbed CO molecule were computed using a semiempirical scheme,[43] as shown in Figure 9C. At the center of the CO molecule, this attractive vdW force is roughly 30% as large as the repulsive electrostatic contribution and improves agreement between theory and experiment, as shown in Figure 9A. While these forces are of the appropriate magnitude and sign to explain the difference between theoretical and experimental scan lines and fall off at the appropriate distance away from the center of the CO molecule, they depend heavily on the height and precise geometry of the nanotip. Since many of our tip parameters are already interdependent, simply correcting for these vdW interactions is difficult. If CO molecules spend more time, on average, in the fully upright configuration than in the tilted configurations, the width of the ring and depth of the depression may differ. These interactions may prove to be of critical importance at shorter tip−sample distances; however, our results clearly demonstrate that at large tip−sample distances good agreement with experiment can be achieved using a simple point dipole model alone.

Tip Sharpness and Resolution. The experimental and theoretical lateral dimensions of CO molecules adsorbed onto NiO(001) are the same size, indicating the presence of an atomically sharp tip apex and negligible tip structure convolution effects. Additionally, the nanotip appears very symmetric as ring height is constant along the entire perimeter. These properties are consistent with the proposed pyramidal tip model. However, this is not always the case as we also observe CO images obtained with blunter and more irregularly shaped tip apexes. In one such example, each surface feature is observed as a double ring, as shown in Figure 10A. Since AFM images are a convolution of the tip and the sample structures, one possible explanation is that the CO molecule on the surface is imaging a multitip instead. This assumption is consistent with experimental images of CO on NiO(001), which suggest that CO molecules do not aggregate. This agrees with our theory since their parallel dipole moments would repel each other on the surface. Within the point dipole approximation, our tip could then be represented by two point dipoles that interact with the CO molecule, as shown in Figure 10B.

In Figure 10A, the two rings are of the same size and height, suggesting that the two point dipoles should be of similar magnitude and positioned at roughly the same height above the surface. The distance between the two rings can be measured from the depression in the center of each one as 0.5 nm. Using this information, an atomistic tip model was proposed for the multitip, as shown in Figure 10C. The structure of this tip model was based on two pyramidal Cr asperities

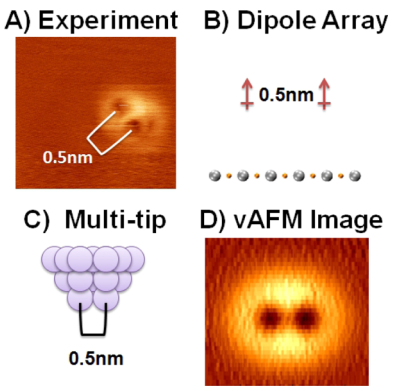

Figure 10. (A) Experimental image of a double ring feature on the surface of NiO(001). The distance between the centers of these two rings is observed to be roughly 0.5 nm. (B) AFM tip collapsed into two point dipoles 0.5 nm apart. (C) Atomistic representation of the Cr nanotip containing two equivalent apex atoms 0.5 nm apart. (D) vAFM image produced using point dipoles positioned at each apex atom. The observed image shows a double ring feature with a distance of 0.5 nm between centers, in agreement with experiment. Experimental parameters: f_0 = 188.334 kHz, c = (147 ± 22) N/m; A = (1.5 ± −0.1) nm, Q = 102361, Δf = −75 Hz.

grown from a Cr(110) surface. It was constructed so that the lateral distance between apex atoms is 0.5 nm, and point dipoles were placed at each of these apex atoms. Theoretical images were then produced using the previously fit set of macroscopic tip parameters, experimental set points, and tip dipole. While these parameters were not fit to this particular set of experimental data, Figure 10D demonstrates good agreement with experiment using a generic point dipole model of the Cr-coated tip.

These results demonstrate how imaging small molecules adsorbed in upright configurations on a surface could be used to characterize the tip structure and confirm that images of adsorbed CO molecules in Figure 8A were indeed obtained with an atomically sharp symmetrical single asperity tip.

Imaging Larger Polar Molecules. Unlike CO-functionalized tips, metallic tips appear unable to image larger molecules with intramolecular resolution in the Pauli repulsion regime on insulators, as the recent studies of Co-Salen molecules on NaCl(001)[28] and NiO(001)[29] indicate. However, since metallic tips possess much larger dipole moments (a few Debye) than CO-functionalized tips (a few 0.1 D), they may be well-suited to probe the dipole moments (or the electrostatic potential) of larger molecules. Co-Salen is a large polar molecule and provides a good example to illustrate this point.

Previous calculations show that the Co-Salen molecule on NiO(001) possesses a 6 D dipole moment aligned along the symmetry axis.[29] The positive end of this dipole moment is oriented toward the N atoms, while the negative end is oriented toward the O atoms. This molecular dipole moment can be visualized using the electrostatic potential of the system from DFT calculations as seen in Figure 11A. The negative

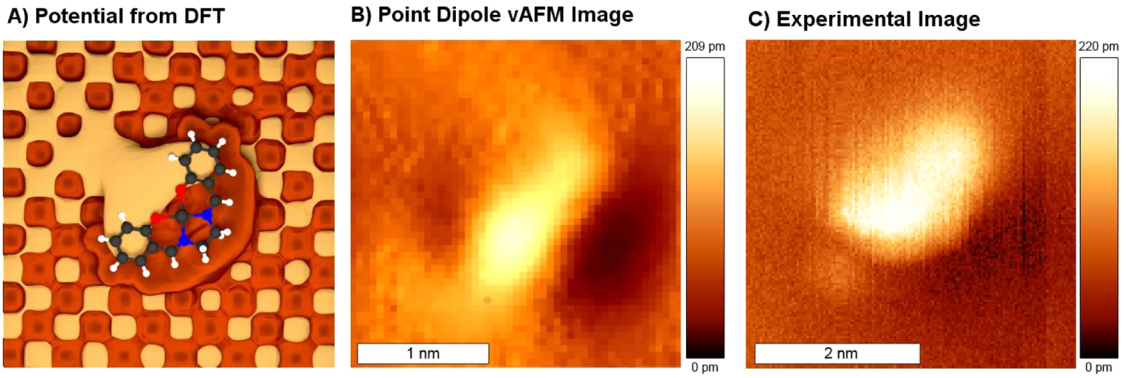

Figure 11. (A) Electrostatic potential of a single Co-Salen molecule adsorbed onto NiO(001). N atoms are shown in blue and O atoms in red. Bright areas represent the negative isosurface (−0.54 eV) where the tip would experience an attractive potential, while dark areas represent the positive isosurface (0.08 eV) or repulsive potential at long distances. (B) vAFM image taken far from the surface. It shows the Co-Salen molecule as a bright oval with a dark shadow on one side. At this range, the metallic-coated Cr tip is unable to distinguish between similar C or H atoms within the molecule. (C) Experimental NC-AFM image of a Co-Salen molecule on NiO(001) taken at long range. Individual Co-Salen molecules do appear as large bright ovals with smaller dark shadows. Experimental parameters: $f_0 = 186.894$ kHz, $Q = 21392$, $A_0 = 5.0 \pm 0.5$ nm, $c = 145 \pm 22$ N/m, $\Delta f = -0.71$ Hz.

isosurface (bright) of the electrostatic potential shows areas where the positive end of a dipole moment would feel an attractive interaction. Experimentally, these areas should result in bright spots in the image. The positive isosurface (dark) highlights areas where the tip would be repelled and should result in dark spots or shadows. Note that the isovalue of the repulsive region (0.08 eV) is much smaller than the attractive region (−0.54 eV), indicating a weaker interaction. A smaller isovalue was used in order to enlarge the repulsive region for the illustration. When adsorbed to NiO(001), the Co-Salen molecule also acquires a 4.4 D vertical dipole moment due to distortion of the molecule and electronic polarization of the system.[29] When this vertical component is added to the horizontal component, the symmetry of the imaged dipole moment is broken. The bright attractive region should now be roughly twice as large as the dark repulsive one, as seen in Figure 11B. Although the atoms within the Co-Salen molecule are not resolved, it may be possible to image the positive and negative lobes of the molecular dipole.

In previous studies of Co-Salen, this imaging mechanism was used to obtain atomic resolution of the NiO surface while the molecule itself was probed at a distance where both Pauli repulsion and electrostatic interactions were present. At such ranges, the bright and dark lobes of the molecule itself could not be consistently identified. However, when Co-Salen molecules are imaged at much greater distances, where the surface atoms are no longer visible, it is possible to resolve the horizontal dipole moment of a Co-Salen molecule, as shown in Figure 11C. The molecule seen in this image consists of a large bright oval and a smaller dark shadow. The shadow appears in both the trace and retrace images, indicating that these dark regions are not due to tip effects. The bright region of the molecule is indeed much larger than the dark repulsive region, which is consistent with theoretical predictions of a tilted total dipole moment on the surface.

DISCUSSION AND CONCLUSIONS

Our experimental results combined with DFT calculations confirm that the Cr tips used in this work possess permanent dipoles with the positive ends oriented toward the sample surface. Long-range vdW interactions between the macrotip and the surface were accounted for by fitting directly to experimental $\Delta f(z)$ curves, which were converted into $F(z)$ curves. The midranged electrostatic interactions were accounted for by considering the interaction between a point dipole located at the tip apex and the electrostatic potential of the sample. On atomically flat polar surfaces, such as NiO(001), the corrugation in the electrostatic potential stems from the periodic arrangement of ions but can also result from the local electric dipole moment of an individual molecule. To demonstrate the feasibility and validity of our point dipole approach, the magnitude and position of a point dipole positioned at the tip apex were fit to experimental scan lines exhibiting atomic resolution on NiO(001) using the vAFM. Using these parameters, we successfully tested our point dipole model on CO molecules adsorbed on NiO(001), which were imaged as donuts using the very same tip. Our method for computing electrostatic interactions is similar to the work of Chelikowsky *et al.*;[47] however, we carefully justify the distance regime and force contribution that is represented in order to produce a quantitative method.

On the basis of these findings, we more generally suggest that atomically sharp metallic tips, either coated Si cantilevers or wire tips, end in a nanoasperity which can be well-described as a pyramid. This greatly reduces the number of possible tip structures that must be considered. In contrast, Si or oxidized Si tips can possess a large number of stable configurations.

Therefore, several likely tip structures must be tested in order to achieve reasonable agreement between theory and experiment.[48] Metallic tip apexes also possess a rather large electric dipole moment of a few Debye that usually points with its positive end toward the surface and can be well-modeled as a point dipole. This property facilitates unambiguous atom identification on polar surfaces at rather large tip−sample separations and substantially reduces the complexity of interpreting experimental data. Moreover, these tip point dipoles may be able to probe the dipole moment of polar molecules on the surface.

Metallic tips may also be functionalized by picking up small molecules such as CO.[21] Such tips have recently been used to obtain intramolecular resolution in the repulsive regime using constant height imaging.[49,50] However, due to the small tip−sample distance and the resulting strong tip−sample interactions in the repulsive regime, image distortions and relaxation effects have to be considered. Since CO possesses an intrinsic dipole moment with its positive pole on the O atom and adsorbs with its C atom onto metal surfaces, it will likely also possess a dipole moment with its positive pole pointing toward the surface. Note that the dipole moment of the metallic nanotip on which CO adsorbs tends to increase the total dipole moment of the adsorbed molecule due to polarization effects. Therefore, CO-functionalized tips can be expected to behave similarly to metal tips, even though their dipole moment is probably smaller. Unfortunately, CO-functionalized tips can be only prepared at low temperatures (otherwise CO is too mobile), and not all sample systems are suitable for CO adsorption.

From a practical point of view, one has to be aware that all tip apexes can become contaminated with sample material during scanning. Therefore, tip changes should be monitored. Whether tip material was lost (the tip becomes shorter) or sample material has been picked up (the tip becomes longer) can be determined by observing the *z*-signal. In the latter case, atom identification on ionic surfaces using metallic tips becomes ambiguous, as the image contrast is determined by the charge state of the foremost tip apex atom. Note that this is true for silicon, silicon oxide, and functionalized tips, as well. However, if a metallic tip picks up nonconductive sample material, the bias spectroscopy curve becomes nonmetallic; that is, the smooth parabola exhibits jumps or hysteresis.[27] In this way, bias spectroscopy provides a convenient *in situ* tool to characterize the state of the metallic tip apex and monitor contamination by nonconductive sample material. If the tip becomes nonmetallic, it can be dipped into a metallic substrate (*e.g.*, Cu) to metallize the tip apex again (voltage pulses are also an option). The use of monitored metallic tips will be advantageous when performing Kelvin probe force microscopy (KPFM) or electrostatic force microscopy (EFM), avoiding the complications of interpretation described by Bieletzki *et al.*[51]

In summary, metallic tips can be conveniently prepared *in situ* and remetallized if they become contaminated. The most stable and thus most likely atomic configuration of the tip apex is a pyramid that possesses a large electric dipole moment of a few Debye with its positive pole pointing toward the surface. This greatly reduces the complexity of interpreting experimental data while allowing for an unambiguous identification of ionic species on polar surfaces at relatively large tip−sample distances. Metallic tips may also be able to detect the electric dipole moments of adsorbed molecules and should be used in KPFM and EFM experiments. It is worth mentioning that, if magnetic metals are used, even magnetic moments can be resolved with atomic resolution.[52,53] In this context, pyramidal nanotips provided excellent agreement between DFT calculations and experimental data regarding the magnitude and distance dependence of the magnetic exchange interaction.[54]

METHODS

Experimental Methods. All measurements were performed at about 8 K with a home-built low-temperature ultrahigh vacuum (UHV) force microscope.[55] The substrate, NiO, crystallizes in the rock salt structure with a lattice constant of 417 pm. Clean (001) surfaces were prepared by *in situ* cleavage of single crystals at a pressure of about 1×10^{-10} hPa and subsequent annealing at about 500 °C to remove residual charges. After cooling the substrate in the cryostat, CO molecules were admitted *via* a leak valve and Co-Salen molecules were evaporated from a crucible. At these low temperatures, both species are immobile, leading to a random distribution of well-separated individual molecules on the surface.

High-resolution AFM measurements were performed in the noncontact mode (NC-AFM) using the frequency modulation technique (FM-AFM).[56] In this mode of operation, the cantilever self-oscillates with constant amplitude A_0 at its resonance frequency f_0. Forces between the tip and sample shift the actual cantilever frequency f by $\Delta f = f - f_0$. To image in the noncontact regime, where attractive forces dominate, a suitable negative Δf was chosen as set point for the *z*-regulator. Scanning the tip line by line across the (x,y) sample surface while Δf is kept constant provides a $z(x,y)$ map of constant tip−sample interaction (*i.e.*, the topography).

To prepare a tip with an electric dipole moment at its apex, supersharp Si cantilevers (2 nm nominal tip radius from www.nanosensors.com) were coated *in situ* with a few nanometers of Cr. The contact potential difference (CPD) between the tip and sample was determined by recording $\Delta f(U_{bias})$ curves. $U_{bias} = U_{CPD}$ was applied between tip and sample to minimize long-range electrostatic interactions. As previously described,[27] these curves were also used to characterize the metal-coated tips.

Density Functional Theory. Investigations of the NiO(001), Cr(110), and Cr(001) surfaces were performed using the CP2K code and the mixed Gaussian and plane wave approach.[57,58] These calculations included geometry minimization and molecular dynamics of the bare surfaces and surfaces with adsorbed single molecules.

Cr surfaces and tip asperities were constructed based on prior experimental studies. Field ion microscopy experiments[20] on W tips show that metal-coated tips may appear spherical and possess (110) terraces near the tip apex. Scanning electron micrographs of sputtered Cr films on SiO_2[36] show that deposited films of Cr may be rough and decorated with a variety of asperities. Using these results, we approximated our Cr-coated tips as macroscopic spheres terminated by (110) terraces decorated by a variety of asperities. Representative nanotips were constructed as pyramidal asperities on the Cr(110) surface, as shown in Figure 1. Asperities on the Cr(001) surface were constructed in the same way. These Cr tip asperities were treated using the PBE/GGA[59,60] functional along with a plane wave cutoff of 350 Ry and the MOLOPT[61] basis set. The basis set was further optimized to produce a 4.8 eV work function for the (110) surface and a 4.0 eV work function for the (001) surface, in good agreement with prior calculations.[27,62]

The dipole moment of these asperities can be calculated by considering the electrostatic potential averaged across the *xy* plane in the two-dimensional periodic cell. The presence of an asperity will shift the vacuum level on either side of the slab and change the work function. This effect can be considered using the parallel plate capacitor model.[63] The work function change is related to the magnitude of the dipole moment and the surface area as follows:

$$\Delta W = \frac{eD}{\varepsilon_0 A} \tag{1}$$

where D is the dipole moment due to the presence of an asperity, A is the area of the system, ε_0 is the electric permittivity of vacuum, and e is the unit of elementary charge.

NiO(001) with adsorbed Co-Salen and CO molecules was treated as previously described.[29] The B3LYP[64,65] hybrid functional was employed in order to describe the NiO surface and the adsorbed molecules to produce a NiO band gap of 3.6 eV compared to an experimental value of 4.3 eV[66] and negligible surface rumpling in agreement with experiment.[67] Additionally, prior calculations suggest that B3LYP is able to produce reasonable bond lengths for the CO molecule on NiO despite a very large basis set superposition error (BSSE). In order to reduce BSSE in our calculations, we employed the MOLOPT[61] basis set and calculated the adsorption energy of CO on NiO(001) to be 0.3 eV, in agreement with prior studies.[44,45] The tilted configuration of CO on NiO was also reproduced with total tilt of 6°.

Finally, in order to mitigate the expense of using a hybrid functional with extensive basis sets, we employed the auxiliary density matrix method.[68] We chose an auxiliary basis set consisting of three uncontracted Gaussians for each angular momentum channel. The auxiliary basis sets for Ni and Co were fit to a set of test molecules, and the basis sets for all other elements were taken from the standard CP2K distribution (pFIT3).[68] The results demonstrate that this basis set and functional produce accurate surface properties and can reasonably represent the adsorbed system, while reducing the BSSE to less than 0.1 eV.

The NiO(001) surface was simulated as a three-layer slab consisting of 288 atoms. The surface size was selected in order to avoid interactions between molecules in the 2D periodic simulation by increasing the size of the cell until the adsorption energy converged. The plane wave cutoff was selected to be 400 Ry by similarly increasing it until adsorption energy converged. A semiempirical correction method[43] was employed to account for long-range dispersion interactions.

Calculating Electrostatic Interactions. If the tip−surface distance is large enough, it is reasonable to assume that the structural deformation of both the metallic tip and the surface can be neglected. However, electronic relaxations may be more significant and need to be considered. Image charges and dipoles, in particular, may contribute significantly to the forces. Fortunately, when studying bulk insulating surfaces, the only image charge that can be induced within our system is the one in the metallic tip by a surface feature. The distance between the image and the surface will be much larger than the distance between the tip apex and the surface resulting in a greatly reduced contribution. The forces resulting from image interactions can be calculated using well-known models as previously described.[69]

For a typical 10 nm radius AFM tip 0.5 nm away from the surface interacting with a feature that possesses a 5 D dipole moment, the image dipole contributes less than 5% of the total midrange forces. Additionally, the tip will only spend a small fraction of the oscillation cycle this close to the surface, further reducing the effect of the image dipole. Since the midrange component is already only a small fraction of the total force, the image contribution is neglected in our model for the sake of simplicity.

The remaining contribution to midrange forces can be attributed to electrostatic interactions between the dipole of the metallic tip and the surface. The AFM tip in this model is approximated as a point dipole far from the surface, and the forces experienced by this tip can be calculated as follows:

$$F_z = \frac{\mathrm{d}}{\mathrm{d}z}\left[D_x\frac{\mathrm{d}V_E}{\mathrm{d}x} + D_y\frac{\mathrm{d}V_E}{\mathrm{d}y} + D_z\frac{\mathrm{d}V_E}{\mathrm{d}z}\right] \tag{2}$$

where F is the normal force felt by the tip, D_{xyz} represents the orientation and magnitude of the dipole moment of the AFM tip, and V_E represents the electrostatic potential of the system at each point of interaction. In the case of blunt tips, the tip structure is represented using an array of point dipoles. The forces experienced by a blunt tip consisting of n dipoles can expressed as follows:

$$F_z = \sum_{i=1}^{n}\frac{\mathrm{d}}{\mathrm{d}z}\left[D_{ix}\frac{\mathrm{d}V_E}{\mathrm{d}x} + D_{iy}\frac{\mathrm{d}V_E}{\mathrm{d}y} + D_{iz}\frac{\mathrm{d}V_E}{\mathrm{d}z}\right] \tag{3}$$

These forces can then be combined with the long-range contribution to generate a complete three-dimensional force field. The final virtual AFM simulations were performed using a previously developed code.[34]

Conflict of Interest: The authors declare no competing financial interest.

Acknowledgment. Financial support from the Deutsche Forschungsgemeinschaft (SFB 668-A5) is gratefully acknowledged. D.Z.G. is grateful to Chevron Oronite Company for financial support. M.B.W. is grateful to the Leverhulme Trust (Grant F/07134/CK) for financial support. The authors acknowledge the use of the HECToR High Performance Computing Facility *via* our membership to the UK's HPC Materials Chemistry Consortium, which is funded by EPSRC (EP/F067496). D.Z.G. acknowledges the use of the Serenity computing cluster and support services provided by Nanolayers.com for the completion of this work.

REFERENCES AND NOTES

1. Besenbacher, F.; Lauritsen, J. V.; Wendt, S. STM Studies of Model Catalysts. *Nano Today* **2007**, *2*, 30–39.
2. Bhalla, G.; Tsang, M. H.; Gao, D.; Chen, Q.; Ruhe, W.; Ushioda, N. Frictional Properties of Molybdenum-Based Lubricating Oil Additives Using Green Chemistry. *SAE Int.* **2012**, *5*, 496–503.
3. Barnes, A. M.; Bartle, K. D.; Thibon, V. R. A. A Review of Zinc Dialkyldithiophosphates (ZDDPS): Characterisation and Role in the Lubricating Oil. *Tribol. Int.* **2001**, *34*, 389–395.
4. Joachim, C.; Gimzewski, J. K.; Aviram, A. Electronics Using Hybrid-Molecular and Mono-Molecular Devices. *Nature* **2000**, *408*, 541–548.
5. Heath, J. R. Molecular Electronics. *Rev. Mater. Res.* **2009**, *39*, 1–23.
6. Song, H.; Reed, M. A.; Lee, T. Single Molecule Electronic Devices. *Adv. Mater.* **2011**, *23*, 1583–1608.
7. Onishi, H.; Sasahara, A.; Uetsuka, H.; Ishibashi, T. A Needle-like Organic Molecule Imaged by Noncontact Atomic Force Microscopy. *Appl. Surf. Sci.* **2002**, *188*, 265–271.
8. Namai, Y.; Fukui, K.; Iwasawa, Y. The Dynamic Behavior of CH_3OH and NO_2 Adsorbed on CeO_2(111) Studied by Noncontact Atomic Force Microscopy. *Nanotechnology* **2004**, *15*, S49–S54.

9. Nony, L.; Bennewitz, R.; Pfeiffer, O.; Gnecco, E.; Baratoff, A.; Meyer, E.; Eguchi, T.; Gourdon, A.; Joachim, C. Cu-TBPP and PTCDA Molecules on Insultating Surfaces Studied by Ultra-High-Vacuum Non-contact AFM. *Nanotechnology* **2004**, *15*, S91–S96.
10. Burke, S. A.; Mativetsky, J. M.; Hoffmann, R.; Grutter, P. Nucleation and Submonolayer Growth of C60 on KBr. *Phys. Rev. Lett.* **2005**, *94*, 096102-1-4.
11. Kunstmann, T.; Schlarb, A.; Fendrich, M.; Wagner, T.; Müller, R. Dynamic Force Microscopy Study of 3,4,9,10-Perylene-tetracarboxylic Dianhydride on KBr(001). *Phys. Rev. B* **2005**, *71*, 121403-1-4.
12. Dienel, T.; Loppacher, C.; Mannfeld, S. C. B.; Forker, R.; Fritz, T. Growth-Mode-Induced Narrowing of Optical Spectra of an Organic Adlayer. *Adv. Mater.* **2008**, *20*, 959–963.
13. Burke, S. A.; Ji, W.; Mativetsky, J. M.; Topple, J.; Fostner, S.; Gao, H. J.; Guo, H.; Grutter, P. Strain Induced Dewetting of a Molecular System: Bimodal Growth of PTCDA on NaCl. *Phys. Rev. Lett.* **2008**, *100*, 7–10.
14. Schutte, J.; Bechstein, R.; Rahe, P.; Kuhnle, A.; Langhals, H. Imaging Perylene Derivatives on Rutile TiO_2(110) by Non-contact Atomic Force Microscopy. *Phys. Rev. B* **2009**, *79*, 045428-1-8.
15. Loske, F.; Bechstein, R.; Schutte, J.; Ostendorf, F.; Reichling, M.; Kuhnle, A. Growth of Ordered C60 Islands on TiO_2(110). *Nanotechnology* **2009**, *20*, 065606-1-5.
16. Kittelmann, M.; Rahe, P.; Kuhnle, A. Molecular Self-Assembly on an Insulating Surface: Interplay between Substrate Templating and Intermolecular Interactions. *J. Phys.: Condens. Matter* **2012**, *24*, 354007-1-5.
17. Hinaut, A.; Pujol, A.; Chaumeton, F.; Martrou, D.; Gourdon, A.; Gauthier, S. An NC-AFM and KPFM Study of the Adsorption of a Triphenylene Derivative on KBr(001). *Beilstein J. Nanotechnol.* **2012**, *3*, 221–229.
18. Hofer, W. A.; Foster, A. S.; Shluger, A. L. Theories of Scanning Probe Microscopes at the Atomic Scale. *Rev. Mod. Phys.* **2003**, *75*, 1287–1331.
19. Pou, P.; Ghasemi, S. A.; Jelinek, P.; Lenosky, T.; Goedecker, S.; Perez, R. Structure and Stability of Semiconductor Tip Apexes for Atomic Force Microscopy. *Nanotechnology* **2009**, *20*, 264015-1-10.
20. Paul, W.; Miyahara, Y.; Grütter, P. Implementation of Atomically Defined Field Ion Microscopy Tip in Scanning Probe Microscopy. *Nanotechnology* **2012**, *23*, 335702-1-7.
21. Gross, L. Recent Advances in Submolecular Resolution with Scanning Probe Microscopy. *Nat. Chem.* **2011**, *3*, 273–278.
22. Schuler, B.; Liu, W.; Tkatchenko, A.; Moll, N.; Meyer, G.; Mistry, A.; Fox, D.; Gross, L. Adsorption Geometry Determination of Single Molecules of Atomic Force Microscopy. *Phys. Rev. Lett.* **2013**, *111*, 106103-1-5.
23. Gross, L.; Mohn, F.; Moll, N.; Schuler, B.; Criado, A.; Guitian, E.; Pena, D.; Gourdon, A.; Meyer, G. Bond-Order Discrimination by Atomic Force Microscopy. *Science* **2012**, *337*, 1326–1329.
24. Ondracek, M.; Pou, P.; Rozsival, V.; Gonzalez, C.; Jelinek, P.; Perez, R. Forces and Currents in Carbon Nanostructures: Are We Imaging Atoms? *Phys. Rev. Lett.* **2011**, *106*, 176101-1-4.
25. Lazo, C.; Caciuc, V.; Holscher, H.; Heinze, S. Role of Tip Size, Orientation, and Structural Relaxations in First-Principles Studies of Magnetic Exchange Force Microscopy and Spin-Polarized Scanning Tunneling Microscopy. *Phys. Rev. B* **2008**, *78*, 214416-1-13.
26. Schwarz, A.; Kaiser, U.; Wiesendanger, R. Towards an Understanding of the Atomic Scale Magnetic Contrast Formation in NC-AFM: A Tip Material Dependent MExFM Study on NiO(001). *Nanotechnology* **2009**, *20*, 264017-1-5.
27. Teobaldi, G.; Lämmle, K.; Trevethan, T.; Watkins, M.; Schwarz, A.; Wiesendanger, R.; Shluger, A. L. Chemical Resolution at Ionic Crystal Surfaces Using Dynamic Atomic Force Microscopy with Metallic Tips. *Phys. Rev. Lett.* **2011**, *106*, 216102-1-4.
28. Lämmle, K.; Trevethan, T.; Schwarz, A.; Watkins, M.; Shluger, A.; Wiesendanger, R. Unambiguous Determination of the Adsorption Geometry of a Metal-Organic Complex on a Bulk Insulator. *Nano Lett.* **2010**, *10*, 2965–2971.
29. Schwarz, A.; Gao, D. Z.; Lämmle, K.; Grenz, J.; Watkins, M.; Shluger, A.; Wiesendanger, R. Determining Adsorption Geometry, Bonding, and Translational Pathways of a Metal-Organic Complex on an Oxide Surface: Co-Salen on NiO(001). *J. Phys. Chem. C* **2013**, *117*, 1105–1112.
30. Smoluchowski, R. Anisotropy of the Electronic Work Function of Metals. *Phys. Rev.* **1941**, *60*, 661–674.
31. Jia, J. F.; Inoue, K.; Hasegawa, Y.; Yang, W. S.; Sakurai, T. Variation of the Local Work Function at Steps on Metal Surfaces Studied with STM. *Phys. Rev. B* **1998**, *58*, 1193–1196.
32. Besocke, K.; Kral-Urban, B.; Wagner, H. Dipole Moments Associated with Edge Atoms; A Comparative Study on Stepped Pt, Au and W Surfaces. *Surf. Sci.* **1977**, *68*, 39–46.
33. Ishida, H.; Liebsch, A. Calculation of the Electronic Structure of Stepped Metal Surfaces. *Phys. Rev. B* **1992**, *46*, 7153–7156.
34. Federici Canova, F.; Foster, A. S.; Rasmussen, M. K.; Meinander, K.; Besenbacher, F.; Lauristen, J. V. Non-contact Atomic Force Microscopy Study of Hydroxyl Groups on the Spinel $MgAl_2O_4$(100) Surface. *Nanotechnology* **2012**, *23*, 1–13.
35. Sun, Z.; Boneschanscher, M. P.; Swart, I.; Vanmaekelbergh, D.; Liljeroth, P. Quantitative Atomic Force Microscopy with Carbon Monoxide Terminated Tips. *Phys. Rev. Lett.* **2011**, *106*, 046104-1-4.
36. Kim, J.; Seo, S.; Park, J.; Lee, J.; Lee, Y.; Ju, B. Effects of Substrate Temperature on Etched Feature of Chromium Film and Its Application to Field Emitter Arrays(FEAs). *J. Korean Phys. Soc.* **2001**, *39*, S101–S107.
37. Liu, C.; Erdmann, J.; Macrander, A. *Thin Solid Films* **1999**, *355−356*, 41–48.
38. Hu, M.; Noda, S.; Okubo, T.; H, K. Wettability and Crystalline Orientation of Cu Nanoislands on SiO_2 with a Cr Underlayer. *Appl. Phys. A: Mater. Sci. Process.* **2004**, *79*, 625–628.
39. Wulff, G. Zur Frage der Geschwindigkeit des Wachstums und der Auflosung der Krystalflachen. *Z. Krystallogr. Mineral.* **1901**, *34*, 449–530.
40. Trevethan, T.; Watkins, M.; Shluger, A. Models of the Interaction of Metal Tips with Insulating Surfaces. *Beilstein J. Nanotechnol.* **2012**, *3*, 329–335.
41. Argento, C.; French, R. H. Parametric Tip Model and Force-Distance Relation for Hamaker Constant Determination from Atomic Force Microscopy. *J. Appl. Phys.* **1996**, *80*, 6081–6090.
42. Bergstrom, L. Hamaker Constants of Inorganic Materials. *Adv. Colloid Interface Sci.* **1997**, *70*, 125–169.
43. Grimme, S. Semiempirical GGA-Type Density Functional Constructed with a Long-Range Dispersion Correction. *J. Comput. Chem.* **2006**, *27*, 1787–1799.
44. Wang, W.; Li, J.; Zhang, Y. The Orbital Interaction of Adsorbed CO on NiO(001;111) Surface: A Periodic Density Functional Theory Study. *Appl. Surf. Sci.* **2006**, *252*, 2673–2683.
45. Rohrbach, A.; Hafner, J.; Kresse, G. *Ab Initio* Study of the (0001) Surface of Hematite and Chromia: Influence of Strong Electronic Correlations. *Phys. Rev. B* **2004**, *70*, 125426-1-13.
46. Kittel, M.; Hoeft, J. T.; Bao, S.; Polcik, M.; Toomes, R. L.; Kang, J.-H.; Woodruff, D. P.; Pascal, M.; Lamont, C. L. A. The Local Adsorption Geometry of CO and NH_3 on NiO(100) Determined by Scanned-Energy Mode Photoelectron Diffraction. *Surf. Sci.* **2002**, *499*, 1–14.
47. Chan, T.-L.; Wang, C. Z.; Ho, K. M.; Chelikowsky, J. R. Efficient First-Principles Simulation of Noncontact Atomic Force Microscopy for Structural Analysis. *Phys. Rev. Lett.* **2009**, *102*, 176101-1-4.
48. Pou, P.; Ghasemi, S. A.; Jelinek, P.; Lenosky, T.; Goedecker, S.; Perez, R. Structure and Stability of Semiconductor Tip Apexes for Atomic Force Microscopy. *Nanotechnology* **2009**, *20*, 264015-1-10.
49. Mohn, F.; Gross, L.; Moll, N.; Meyer, G. Imaging the Charge Distribution within a Single Molecule. *Nat. Nanotechnol.* **2012**, *7*, 227–231.

50. Liljeroth, P.; Repp, J.; Meyer, G. Current-Induced Hydrogen Tautomerization and Conductance Switching of Naphthalocyanine Molecules. *Science* **2007**, *317*, 1203–1206.
51. Bieletzki, M.; Hynninen, T.; Soini, T. M.; Pivetta, M.; Henry, C. R.; Foster, A. S.; Esch, F.; Barth, C.; Heiz, U. Topography and Work Function Measurements of Thin MgO(001) Films on Ag(001) by NC-AFM and KPFM. *Phys. Chem. Chem. Phys.* **2010**, *12*, 3203–3209.
52. Kaiser, U.; Schwarz, A.; Wiesendanger, R. Magnetic Exchange Force Microscopy with Atomic Resolution. *Nature* **2007**, *446*, 522–525.
53. Granovskij, M.; Schron, A.; Bechstedt, F. Magnetic Exchange Force Microscopy from First Principles: Application to the Antiferromagnetic NiO(001) Surface. *New J. Phys.* **2014**, *16*, 023020-1-18.
54. Schmidt, R.; Lazo, C.; Kaiser, U.; Schwarz, A.; Heinze, S.; Wiesendanger, R. Quantitative Measurement of the Magnetic Exchange Interaction across a Vacuum Gap. *Phys. Rev. Lett.* **2011**, *106*, 257202-1-4.
55. Liebmann, M.; Schwarz, A.; Langkat, S. M.; Wiesendanger, R. A Low-Temperature Ultrahigh Vacuum Scanning Force Microscope with a Split-Coil Magnet. *Rev. Sci. Instrum.* **2002**, *73*, 3508–3514.
56. Albrecht, T. R.; Grütter, P.; Horne, D.; Rugar, D. Frequency Modulation Detection Using High-Q Cantilevers for Enhanced Force Microscope Sensitivity. *J. Appl. Phys.* **1991**, *69*, 668–673.
57. Lippert, G.; Hutter, J.; Parrinello, M. A Hybrid Gaussian and Plane Wave Density Functional Scheme. *Mol. Phys.* **1997**, *92*, 477–487.
58. VandeVondele, J.; Krack, M.; Mohamed, F.; Parrinello, M.; Chassaing, T.; Hutter, J. QUICKSTEP: Fast and Accurate Density Functional Calculations Using a Mixed Gaussian and Plane Waves Approach. *Comput. Phys. Commun.* **2005**, *167*, 103–128.
59. Perdew, J. P.; Burke, K.; Ernzerhof, M. Generalized Gradient Approximation Made Simple. *Phys. Rev. Lett.* **1996**, *77*, 3865–3868.
60. Perdew, J. P.; Burke, K.; Ernzerhof, M. Generalized Gradient Approximation Made Simple. *Phys. Rev. Lett.* **1997**, *78*, 1396.
61. VandeVondele, J.; Hutter, J. Gaussian Basis Sets for Accurate Calculations on Molecular Systems in Gas and Condensed Phases. *J. Chem. Phys.* **2007**, *127*, 114105-1-9.
62. Ossowski, T.; Kiejna, A. Density Functional Study of Surface Properties of Chromium. *Surf. Sci.* **2008**, *602*, 517–524.
63. Jackson, J. *Classical Electrodynamics*; Wiley, New York, 1998.
64. Becke, A. D. Density Functional Thermochemistry. III. The Role of Exact Exchange. *J. Chem. Phys.* **1993**, *98*, 5648–5652.
65. Stephens, P. J.; Devlin, F. J.; Chabalowsky, C. F.; Frisch, M. J. *Ab Initio* Calculation of Vibrational Adsorption and Circular Dichroism Spectra Using Density Functional Force Fields. *J. Phys. Chem.* **1994**, *98*, 11623–11627.
66. Sawatzky, G. A.; Allen, J. W. Magnitude and Origin of the Band Gap in NiO. *Phys. Rev. Lett.* **1984**, *53*, 2339–2342.
67. Castell, M. R.; Dudarev, S. L.; Muggelberg, C.; Sutton, A. P.; Briggs, G. A. D.; Goddard, D. T. Surface Structure and Bonding in the Strongly Correlated Metal Oxides NiO and UO_2. *J. Vac. Sci. Technol.* **1998**, *16*, 1055–1058.
68. Guidon, M.; Hutter, J.; VandeVondele, J. Auxiliary Density Matrix Methods for Hartree-Fock Exchange Calculations. *J. Chem. Theory Comput.* **2010**, *6*, 2348–2364.
69. Kantorovich, L.; Livshits, A. I.; Stoneham, M. Electrostatic Energy Calculation for the Interpretation of Scanning Probe Microscopy Experiments. *J. Phys.: Condens. Matter* **2000**, *12*, 795–814.